Available online at www.sciencedirect.com

ScienceDirect

IFAC PapersOnLine 54-16 (2021) 307–313

Maximum A Posteriori estimation for AUV localization with USBL measurements ⋆

Matteo Franchi [*,***] **Alessandro Bucci** [*,***]
Leonardo Zacchini [*,***] **Alessandro Ridolfi** [*,***]
Matteo Bresciani [**,***] **Giovanni Peralta** [**,***]
Riccardo Costanzi [**,***]

[*] *Department of Industrial Engineering, University of Florence, via di Santa Marta 3, 50139, Florence, Italy*
[**] *Dipartimento di Ingegneria dell'Informazione (DII), Università di Pisa, Largo Lucio Lazzarino 1, 56122, Pisa, Italy*
[***] *Interuniversity Center of Integrated Systems for the Marine Environment (ISME), www.isme.unige.it*

Abstract: Due to the limitations of electromagnetic signals, underwater scenarios increase the complexity of developing accurate navigation systems. In the last decades, Ultra-Short BaseLine (USBL) positioning systems have been widely and efficiently used for Autonomous Underwater Vehicles (AUVs) localization, endorsing to be a suitable solution to limit the navigation drift without requiring periodic surfacing for Global Positioning System (GPS) resets. Typically, in the localization context, USBL measurements are exploited as observations within the on-board navigation filter where, most of the time, Extended Kalman Filter (EKF) or Unscented Kalman Filter (UKF) solutions are employed. In a break-away from the above-mentioned approaches, in this study, the localization task is solved as a Maximum A Posteriori (MAP) estimation problem. The presented solution is validated through the use of data gathered in October 2020 during EUMarineRobots (EUMR) tests in La Spezia (Italy) within the activities of the SEALab, the joint research laboratory between the Naval Support and Experimentation Center (Centro di Supporto e Sperimentazione Navale, CSSN) of the Italian Navy and the Interuniversity Center of Integrated Systems for the Marine Environment (ISME).

Keywords: Autonomous Underwater Vehicles, marine system navigation, data-fusion, field robotics, localization.

1. INTRODUCTION

In the last few years, the employment of Autonomous Underwater Vehicles (AUVs) to perform dangerous and challenging missions has widely increased. Possible application fields cover various areas of interest, from environment monitoring to industrial and military operations. Furthermore, the demanded tasks for underwater operations have become more challenging, leading to the development of AUVs capable of performing interactive tasks, such as maintenance and repair of seabed installations (Cieslak et al., 2015) or unknown environment mapping (Vidal et al., 2019). Consequently, the design of a high-accuracy and robust navigation system is a mandatory requirement to perform autonomous underwater missions.

Due to the limitations of electromagnetic signals, underwater scenario poses relevant issues on developing an accurate navigation system. The localization drift, which negatively influences the achievement of the mission goals, has to be bounded with periodic resurfacing operations to obtain Global Positioning System (GPS) resets or with the employment of acoustic-based solutions, such as the Long BaseLine (LBL) and the Ultra-Short BaseLine (USBL) (Leonard and Bahr, 2016). As far as USBL is concerned, previous works typically exploit Kalman Filter techniques. While in Font et al. (2017) the authors present a two-parallel Extended Kalman Filter (EKF) solution which fuses the measurements provided by the vehicle on-board sensors with the ones acquired by the USBL, in Morgado et al. (2011) a linear time-varying Kalman filter is employed for integrated USBL-Inertial Measurement Unit (IMU) navigation. Wang et al. (2020) present a Strap-Down Inertial Navigation System (SINS)/USBL in robust Kalman filter framework. In Kim (2020), in a multi-AUV context, the author employs an Unscented Kalman Filter (UKF)/EKF fusion strategy to estimate both the navigation state and the unknown marine currents. Furthermore, on-field localization experimental tests are reported in Caiti et al. (2014) and Costanzi et al. (2017). In a break-away from the above-mentioned approaches, Maximum A Posteriori (MAP) estimation for AUV localization in the presence of USBL observations is detailed in this work. Beginning from the seminal works of Lu and Milios (1997) and Gutmann and Konolige (1999), MAP estimation has recently become the standard approach for modern Simultaneous Localization and Mapping (SLAM) strategies (Cadena et al.,

⋆ The research leading to these results has been partially supported by the European project EUMarineRobots (EUMR), which received funding from the European Unions Horizon 2020 research and innovation program under grant agreement No 731103.

10.1016/j.ifacol.2021.10.109

2016). Indeed, while fixed-lag smoothers and filtering solutions restrict the inference within a window of the latest states or to the latest state, respectively, MAP strategies estimate the entire history of the system by solving a nonlinear optimization problem. Both fixed-lag smoothers and filters marginalize older states, collapsing the corresponding information (usually) in a Gaussian prior. This approach can lead to reduced robustness against outlier data (Forster et al., 2016). Since MAP strategies can quickly lead to an unsuitable approach for real-time applications, the development of incremental smoothing techniques has arisen as the state-of-the-art approach. Such techniques can reuse previously calculated quantities when new measurements or variables are added (Kaess et al., 2008), (Kaess et al., 2012). Kaess et al. (2012) employs a Bayes tree data structure to perform incremental optimization on the factor graph. Also, the adopted solution possesses the ability to identify and update only a small subset of variables by accurately selecting the ones affected by the new measurement. A complete review can be found in Grisetti et al. (2020) and the references therein.
While filtering approaches for AUVs localization in the presence of USBL measurements have been in-depth analyzed (such as, to name a few, EKF and UKF), MAP estimation still represents an interesting field of research. Specifically, the main contributions of this work are:

- the development of a MAP estimator tailored to AUV localization in the presence of USBL observations;
- the post-processing validation of the presented solution through the use of real data gathered during at sea experiments. In detail, within the positional part of the here presented MAP estimator, a simplified dynamic motion model is employed together with USBL and Depth Sensor (DS) observations;
- the evaluation of the presented approach both in terms of localization accuracy and computational burden. As far as localization performance is concerned, a Doppler Velocity Log (DVL)-based Dead Reckoning (DR) strategy is employed as a benchmark.

The paper is organized as follows: the data acquisition process is detailed in Section 2, whereas Section 3 involves the MAP estimation theory. Section 4 is dedicated to the description of the here presented strategy. Last, Section 5 draws conclusions.

2. DATA ACQUISITION

A data acquisition campaign took place at sea in La Spezia (Italy) within the activities of the SEALab, the joint research laboratory between the Naval Support and Experimentation Center (Centro di Supporto e Sperimentazione Navale, CSSN) of the Italian Navy and the Interuniversity Center of Integrated Systems for the Marine Environment (ISME) in October 2020. The operational area is an artificial basin confined between two piers. The depth within the basin ranges from 3 m to 15 m. Thus, due to the very shallow water, the scenario is challenging from an acoustic point of view. The marine robotics assets involved two heterogeneous vehicles, namely an AUV and an Autonomous Surface Vehicle (ASV). The former is FeelHippo AUV, a lightweight vehicle developed by the Department of Industrial Engineering of the University of Florence (UNIFI DIEF). In contrast, the latter is Mobile Gateway Buoy 300 (MGB300), a torpedo-shape ASV designed and realized by the Italian company Graal Tech Srl. The main physical characteristics of FeelHippo AUV, together with its localization-related sensors are listed in Tab.1. Concerning MGB300, specific information is not available. However, a GPS, an IMU, and an USBL are installed on board.

Table 1. FeelHippo AUV main characteristics and sensor-set.

Physical characteristics

Autonomy [h]	2-3
Controlled DOFs	4
Max. longitudinal speed [m/s]	1.0
Max. lateral speed [m/s]	0.2
Max. depth [m]	30.0
Dimensions [m]	0.6×0.64×0.5
Dry mass [kg]	35

Main sensors

IMU	Orientus Advanced Navigation
Fiber Optic Gyroscope (FOG)	KVH DSP 1760
DVL	Nortek DVL1000 DVL
GPS	U-blox NEO-7P
Depth Sensor (DS)	integrated within the DVL
Acoustic modem	EvoLogics S2CR 18/34

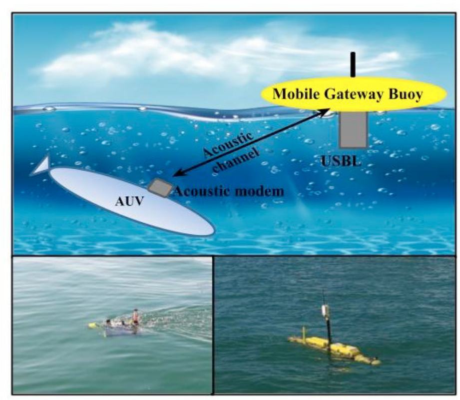

Fig. 1. The test architecture, where Mobile Gateway Buoy MGB300 (lower right image) and FeelHippo AUV (lower left image) are involved, is reported in the upper figure.

Turning to a more detailed description of the accomplished experimental test, MGB300 was hovering on a fixed point on the surface, and FeelHippoAUV performed an autonomous lawnmower path at a constant depth of 4 m. In order to reduce the acoustic noise produced by the thrusters mounted on FeelHippo AUV, the desired longitudinal cruise speed was set at a low value (0.2 m/s). The vehicle navigated resorting to a simple DR strategy, where DVL readings were integrated exploiting the attitude estimator developed by the authors in Costanzi et al. (2016). Meanwhile, MGB300 ASV was able to actively localize (with respect to itself) FeelHippo AUV during the mission exploiting the USBL device installed on board. Moreover, combining the GPS signal and the attitude information coming from the IMU integrated within the

USBL device, MGB300 was able to compute the position of FeelHippo AUV in geodetic coordinates. Such coordinates, at which a unique ID is assigned, were sent to the AUV via the underwater acoustic channel. Thanks to a specifically designed communication protocol, the AUV was able to associate the received position measurement to the correct acquisition time. Furthermore, by exploiting the same communication channel, the protocol allowed transmitting messages necessary to control and monitor the AUV. Fig.1 depicts the described ASV-AUV architecture and it shows the two vehicles during these experiments at sea.

3. MAXIMUM A POSTERIORI ESTIMATION

MAP estimation provides the most likely state set $\mathbf{x} = \{\mathbf{x}_1, \mathbf{x}_2, ..., \mathbf{x}_M\}$ of the modeled system given a set of measurements $\mathbf{z} = \{\mathbf{z}_1, \mathbf{z}_2, ..., \mathbf{z}_N\}$. This problem can be graphically represented using factor graphs (Kschischang et al., 2001), (Dellaert et al., 2017). A factor graph is a bipartite graph that possesses two types of nodes: variables and factors. Assuming the conditional independence of measurements, which is encoded in the connectivity of the factor graph, the MAP estimation problem can be formulated as:

$$\mathbf{x}^* = \underset{\mathbf{x}}{\operatorname{argmax}}\ p(\mathbf{x}) \prod_{i=1}^{N} p(\mathbf{z}_i|\mathbf{x}) \tag{1}$$

where $p(\mathbf{z}_i|\mathbf{x})$ is the likelihood distribution. It is worth noting that in general $\mathbf{z}_i$ is conditioned on a subset of the variables $\subseteq \mathbf{x}$. For what concern the likelihood distribution, as reported in Eq.2, an additive Gaussian noise is assumed in all measurements models.

$$p(\mathbf{z}_i|\mathbf{x}) = \mathcal{N}(\mathbf{h}_i(\mathbf{x}), \Sigma_i) \tag{2}$$

where $\mathbf{h}_i(\mathbf{x})$ is the measurement function, which maps the state estimate $\mathbf{x}$ into a predicted value $\hat{\mathbf{z}}_i$ of the measurement $\mathbf{z}_i$. Instead, Σ_i is the covariance matrix, which summarizes the uncertainty of the measurement model. Under these assumptions, the MAP estimation can be simplified in a non-linear least squares problem:

$$\mathbf{x}^* = \underset{\mathbf{x}}{\operatorname{argmin}}\ \sum_{i=1}^{N} \|\mathbf{h}_i(\mathbf{x}) - \mathbf{z}_i\|^2_{\Sigma_i} \tag{3}$$

where

$$\|\mathbf{h}_i(\mathbf{x}) - \mathbf{z}_i\|^2_{\Sigma_i} = (\mathbf{h}_i(\mathbf{x}) - \mathbf{z}_i)^\top \Sigma_i^{-1} (\mathbf{h}_i(\mathbf{x}) - \mathbf{z}_i) \tag{4}$$

is the Mahalanobis distance.

The non-linear problem can be solved through standard methods, such as the Gauss-Newton or Levenberg-Marquardt algorithms, which iteratively converge to the solution by solving the linear approximation of the non-linear system. Given an initial state estimate $\mathbf{x}^0$, the linearized measurement equation is:

$$\mathbf{h}_i(\mathbf{x}) = \mathbf{h}_i(\mathbf{x}^0 + \Delta\mathbf{x}) \approx \mathbf{h}_i(\mathbf{x}^0) + \left.\frac{\partial \mathbf{h}_i(\mathbf{x})}{\partial \mathbf{x}}\right|_{\mathbf{x}^0} \Delta\mathbf{x} \tag{5}$$

where $\Delta\mathbf{x} = \mathbf{x} - \mathbf{x}^0$ is the state update. Substituting this approximation in Eq.3, the system can be solved in terms of the variable $\Delta\mathbf{x}$. The current update $\Delta\mathbf{x}^*$ is employed to propagate the estimation, whose value is used as linearization point for the next algorithm step. More information can be found in Grisetti et al. (2020).

The above optimization is valid when the state is defined over an Euclidean domain. However, as detailed in Section 4, the presented MAP estimation problem is defined over elements of $SE(3)$, leading to an optimization problem that involves quantities that live on a smooth manifold. A complete treatment goes beyond the scope of this study and more information can be found in Absil et al. (2007) and Chirikjian (2011).

4. PROBLEM DEFINITION AND POST-PROCESSING VALIDATION

The details concerning the estimator are given in Section 4.1, whereas the results are described in Section 4.2. Last, in Section 4.3, a brief computational burden analysis is shown.

4.1 Problem definition

The state of the system at instant i is defined as a complete pose $\in SE(3)$. Mathematically:

$$T_{x_i} = \begin{bmatrix} R_i & \mathbf{t}_i \\ \mathbf{0}^\top & 1 \end{bmatrix} \mid R_i \in SO(3), \mathbf{t}_i \in \mathbb{R}^3, \tag{6}$$

where R is the rotation matrix and $\mathbf{t}$ represents the translation part. The optimization on smooth manifold, such as $SE(3)$ elements is implemented in the GTSAM library, employed as back-end for the localization problem (Dellaert, 2012). Let us define the set of poses at time k with $\mathcal{X}_k$, such that $\mathcal{X}_k = \{T_{x_i}\}_{i=0,...,k}$. Considering a transformation from x_i to x_j with covariance $\Sigma_{i,j}$, and constrained with a measurement $z_{i,j}$, Eq.4 for $SE(3)$ elements becomes $\left\| Log\left(T_{z_{i,j}}^{-1} T_{x_i}^{-1} T_{x_j}\right)\right\|^2_{\Sigma_{i,j}}$. In contrast, for a measurement z_i that indicates a pose prior on x_i with covariance Σ_i, Eq.4 is $\left\| Log\left(T_{z_i}^{-1} T_{x_i}\right)\right\|^2_{\Sigma_i}$. $Log(\cdot)$ maps from the manifold to an element of the $SE(3)$ Lie Algebra where, for the sake of brevity, a minimal vectorized representation is used to describe an element of the Lie Algebra. The above-mentioned logarithmic map and the exponential map are discussed in Wang and Chirikjian (2008), and Dellaert et al. (2017). The presented MAP estimator can resort to:

- DS measurements at an approximate frequency of 4 Hz;
- GPS data at 10 Hz and USBL observations at non-fixed frequency;
- Roll, Pitch and Yaw (RPY) information provided at 10 Hz by the attitude estimator developed in Costanzi et al. (2016);
- a simplified dynamic model of the AUV motion (as described in the authors' previous work Franchi et al. (2020)) available at 10 Hz that provides an estimate of the vehicle speed.

The above-mentioned information has been encoded as measurement factors to constraint the optimization, whose solution represents the MAP estimate. Inspired by Westman and Kaess (2019), the following factors have been included:

- a relative 4D pose-to-pose constraint on x, y, and z translation and yaw rotation, denoted as XYZ − Y;
- an unary 2D constraint on pitch and roll rotations, indicated as RP;

- an unary 1D constraint on z translation, represented with Z;
- an unary constraint on x and y translation exploiting GPS and USBL observations, denoted as $\mathrm{XY_{GPS}}$ and $\mathrm{XY_{USBL}}$, respectively.

A naive implementation of the estimator would consist in adding a state node at the frequency of the attitude estimator and the model (10 Hz), leading to a waste of resources. The implemented approach adds a new state only when at least one observation from USBL, GPS or DS is available. The link between adiacent nodes is maintained by collapsing the relative motion XYZ-Y in a single compound constraint, where simple DR is performed between the two consecutive nodes. A graphical representation of the factor graph is given in Fig.2. For

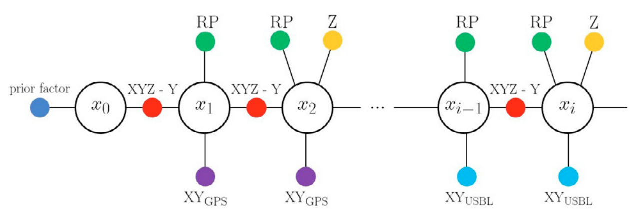

Fig. 2. The factor graph employed to constraint the optimization. It can be noted how a new state is added only when at least one observation from USBL, GPS, or DS is available.

the ease of explanation, let us represent a pose T_{x_i} with a vector $[X_{x_i}, Y_{x_i}, Z_{x_i}, \phi_{x_i}, \theta_{x_i}, \psi_{x_i}]^\top \in \mathbb{R}^6$ that encodes the state at the generic instant. Mathematically, at time k, the optimization problem can be written as:

$$
\begin{aligned}
\mathcal{X}_k^* = \underset{\mathcal{X}_k}{\operatorname{argmin}} \sum_{i=1}^{k-1} (&\underbrace{\| f(x_{i-1}, x_i) \ominus o_{i-1,i} \|^2_{\Sigma_{o_{i-1,i}}}}_{\text{XYZ}-\text{Y factor}} \\
&+ \underbrace{\| g(x_i) \ominus r_i \|^2_{\Sigma r_i}}_{\text{RP factor}}) \\
&+ \sum_{i \in \mathcal{Z}} \underbrace{\| h(x_i) - z_i \|^2_{\Sigma z_i}}_{\text{Z factor}} + \sum_{i \in \mathcal{U}} \underbrace{\| l(x_i) - \mathbf{u}_i \|^2_{\Sigma u_i}}_{\mathrm{XY_{USBL}} \text{ factor}} \\
&+ \sum_{i \in \mathcal{G}} \underbrace{\| l(x_i) - \mathbf{g}_i \|^2_{\Sigma g_i}}_{\mathrm{XY_{GPS}} \text{ factor}} + \underbrace{\left\| T_{x_0} \ominus T_{x_{prior}} \right\|^2_{\Sigma_0}}_{\text{prior factor}} .
\end{aligned}
\tag{7}
$$

$\{f(\cdot), \Sigma_{o_{i-1,i}}\}, \{g(\cdot), \Sigma_{r_i}\}, \{h(\cdot), \Sigma z_i\}, \{l(\cdot), \Sigma_{u_i}\}, \{l(\cdot), \Sigma_{g_i}\}$ are the measurement function and covariances associated to the $\mathrm{XYZ-Y}$, RP, Z, $\mathrm{XY_{USBL}}$, and $\mathrm{XY_{GPS}}$ factors, respectively. $\mathcal{Z}$, $\mathcal{U}$, $\mathcal{G}$ are the set of nodes for which DS, USBL, and GPS measurements occur, respectively. $T_{x_{prior}}$ is the prior on the first pose, which is necessary to anchor the state evolution to a global coordinate frame. $o_{i-1,i}$ and r_i represent, on $SE(3)$, the observations for the XYZ-Y and RP part, respectively, $z_i \in \mathbb{R}$ is the depth measurement, and $\mathbf{u}_i \in \mathbb{R}^2$, $\mathbf{g}_i \in \mathbb{R}^2$ are the USBL and GPS observations, respectively. Last, $\ominus$ encodes the logarithmic map of the relative transformation between $SE(3)$ elements $\left\| Log\left(T^{-1}_{x_{prior}} T_{x_0}\right) \right\|^2_{\Sigma_0}$. In Eq.7, the measurement functions are:

$$
\begin{aligned}
f(x_{i-1}, x_i) &= \left[\, X_{x_{i-1,i}} \;\; Y_{x_{i-1,i}} \;\; Z_{x_{i-1,i}} \;\; \psi_{x_{i-1,i}} \,\right]^\top \\
g(x_i) &= \left[\, \phi_{x_i} \;\; \theta_{x_i} \,\right]^\top \\
h(x_i) &= \left[\, Z_{x_i} \,\right]^\top \\
l(x_i) &= \left[\, X_{x_i} \;\; Y_{x_i} \,\right]^\top
\end{aligned}
\tag{8}
$$

Generally speaking, USBL observations are not immediately available for the localized vehicle. However, by streaming the absolute acquisition time together with the absolute coordinates, the USBL message, once available, can be adequately accounted. To this end, the association is performed by finding the nearest node on the graph to the current USBL observation. The distance is evaluated by looking at the absolute time of each node in the graph. Given the average rate of the DS, which is around 4 Hz, and considering the low dynamics involved, the presented strategy seems sufficient for this study. In addition to this, it is well-known that USBL observations can typically present outliers. Therefore, an outlier rejection step is fundamental. In this study, the Mahalanobis distance between the measurement and its expected value is considered:

$$
\| \hat{\mathbf{z}}_{USBL} - \mathbf{u}_i \|^2_{\Sigma_i}, \tag{9}
$$

where $\mathbf{u}_i \in \mathbb{R}^2$ is the USBL observation acting on node x_i, $\hat{\mathbf{z}}_{USBL} \in \mathbb{R}^2$ is its expected value, and Σ_i is the associated covariance calculated as $\Sigma = H\Sigma_{x_i}H^T + \Sigma_{u_i}$. Σ_{x_i} represents the marginal covariance of the associated state, H encodes the measurement model (which is linear in this study), and Σ_{u_i} is the measurement covariance. It can be shown that in the Gaussian case, Eq.9 follows a χ^2_ς distribution with $\varsigma = dim(\mathbf{u}_i) = 2$ that denotes the degrees of freedom. If the measure is consistent, given a confidence level of 95 %, the one-side acceptance region for Eq.9 becomes $[0; 5.99]$ In other context, the following test is known as Normalized Innovation Squared (NIS) test (Bar-Shalom et al., 2004).

4.2 Post-processing validation

The real data acquired with the setup described in Section 2 have been used as input to implement the estimator delineated in Section 3. Concerning the implementation, a C++ Robot Operating System (ROS) (Quigley et al., 2009) architecture has been employed with the GTSAM library (Dellaert, 2012) as back-end for localization solution. More information can be found in Kaess et al. (2008), Kaess et al. (2012). iSAM2, which is the last evolution of the incremental smoothing and mapping solution developed in GTSAM, permits to identify and update only the small subset of variables affected by a new measurement, which is typically small, and therefore to limit the computational burden of the estimation, offering a trade-off between accuracy and efficiency. Some remarkable iSAM2 real-worlds implementation in the robotics field can be found in Forster et al. (2016) and Westman and Kaess (2019).

In order to evaluate the performance of the here presented localization solution, the DR strategy employed by FeelHippo AUV during the underwater tests has been used as benchmark. It is worth pointing out that while on the surface, FeelHippo AUV resorted to raw GPS fixes. Although the DR strategy is prone to accumulate drift over time (being not an absolute ground-truth), for short missions, due to the presence of top-of-the-line sensors (the single-axis FOG and the DVL), the strategy can be deemed as a reasonable benchmark. In the following, the DR strategy (with GPS fixes when the vehicle is on the surface) will be identified as Benchmark Path (BP).

With regards to localization accuracy, the following metrics have been employed:

$$e_i = \left\| \boldsymbol{\eta}_{1_{BP_i^{x,y}}} - \boldsymbol{\eta}_{1_{MAP_i^{x,y}}} \right\| \tag{10}$$

$$\bar{e}_k = \frac{\sum_{i=0}^{i=k-1} e_i}{k}, \tag{11}$$

where $e_i \in \mathbb{R}^+$ is, at the instant $i \in \mathbb{N}$, the navigation error in the horizontal plane; indeed, the presence of the DS provides direct measurements of the depth both for DR and MAP strategy; therefore, the study on vertical direction can be neglected. $\boldsymbol{\eta}_{1_{BP_i^{x,y}}}$ and $\boldsymbol{\eta}_{1_{MAP_i^{x,y}}}$ indicate the position of the vehicle on the horizontal plane according to the BP and to the MAP estimator, respectively. In addition to this, $\bar{e}_k \in \mathbb{R}^+$ indicates the mean of e_i for $i = 0, ..., k-1$. The results are depicted in Fig.3 and Fig.4 and are summarized in Tab.2. In order to provide more

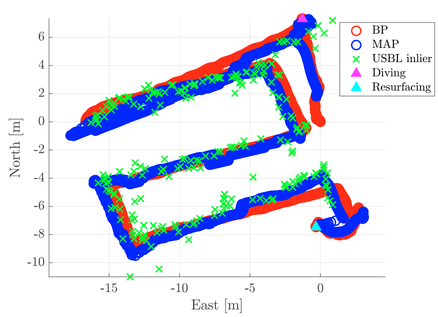

Fig. 3. The navigation results. In red, the BP, whereas in blue the proposed MAP estimator. Last, in green, the USBL measures considered as inliers.

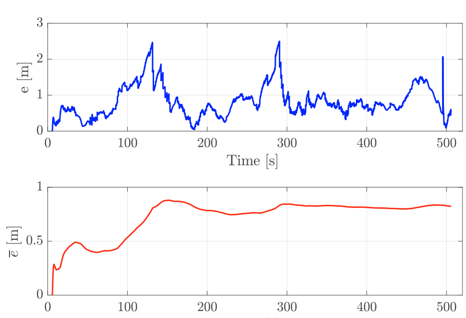

Fig. 4. Quantitative evaluation of the MAP estimator. In the top figure (in blue), the error defined in Eq.10 is depicted. The spike around 500 s on the quantity defined in Eq.10 is due to the resurfacing. In contrast, in the bottom figure (in red), the error defined in Eq.11 is presented. It can be easily noted how the evolution of the error remains bounded thanks to USBL observations.

insights on the evolution of the localization performance during the mission, the metric in Eq.10 has been evaluated in five different sub-trajectories (equally spaced) of the

Table 2. Navigation performance. "Max. error" is the maximum of the metrics in Eq.10 during the underwater mission. "Mean error" is the mean as detailed in Eq.11 and calculated before resurfacing. "Res. error" is the distance (in the horizontal plane) between the last position estimated while the vehicle is underwater and the first GPS position after resurfacing.

Max. error [m]	**Mean error [m]**	**Res.error [m]**
2.499 (@290.6 s)	(0.833 @resurfacing)	2.045

overall mission. To better catch the behaviour in each sub-trajectory, an alignment translation has been computed from the first state and the corresponding benchmark of each sub-trajectory. The final results are presented in Fig.5.

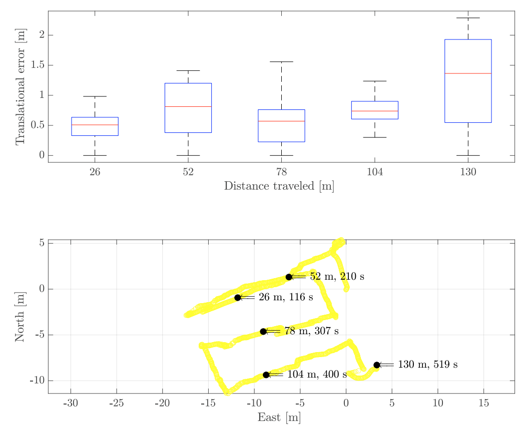

Fig. 5. In the top figure, the error in Eq.10 is shown as a series of boxplots for different sub-trajectories. The box in the middle indicates the 25th and 75th percentiles of the sample, respectively, and the red line the median. Last, the whiskers identify, away from the bottom or the top of the box, the most extreme data values below 1.5 times the interquartile range. In the bottom figure, the navigation path for the MAP estimator where the points corresponding to the traveled distance are made evident. The mission time for those points is provided as well.

4.3 Computational burden analysis

As far as the computational burden is concerned, the following points have been subject matter of the research (it is worth highlighting that the simulations have been performed on a laptop PC i7-6700HQ CPU@2.60GHz with 16 GB RAM):

- the execution time of the localization estimator, calculated at each step;
- the CPU burden;
- the memory burden.

Concerning the CPU and memory burden, the output of the command *top*, which is a task manager program present in many Unix-like operating systems that provides a dynamic real-time view of a running system, has been

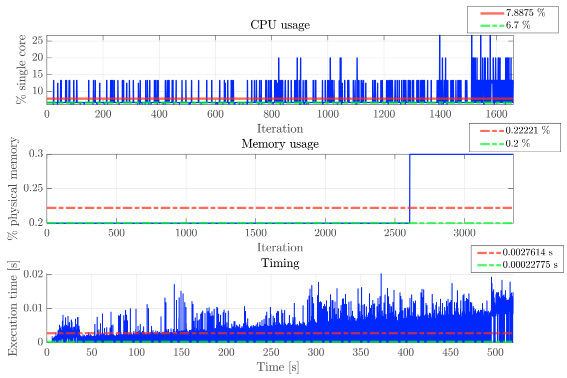

Fig. 6. Computational burden analysis. In red and green are indicated the mean and the median, respectively. Concerning the CPU usage, when the *top* call provided zero output, the value was not stored.

recorded and stored around every 0.15 s. The results are visible in Fig.6. It can be noted how the required resources are limited for the employed laptop PC, suggesting the feasibility for online tests on common AUV platforms.

5. CONCLUSIONS AND FUTURE WORKS

In the presented work, a MAP estimator tailored to AUV localization in the presence of USBL measurements has been developed and tested in post-processing. The validation has been accomplished by employing a DVL-based DR approach used as a benchmark. Turning to the navigation performance analysis, the presented solution has shown a promising localization behavior. In particular, the maximum horizontal error with respect to the BP results around 2.5 m; in contrast, GPS fixes obtained after resurfacing indicate an absolute error of around 2 m. Furthermore, an analysis of the computational burden has been undertaken, and its results suggest the feasibility for online tests on common AUV platforms.

Future works will consist in employing raw data from on-board attitude sensors (such as IMU and FOG), and information from perceptual devices within the MAP estimator. Moreover, on-line tests at sea will be performed shortly to validate the hereby proposed approach. In this context, the authors will plan *ad-hoc* missions, where absolute positioning measurements (*e.g.*, from the GPS) could help to evaluate better the performance of the method.

ACKNOWLEDGEMENTS

The authors would like to thank all the SEALab members, the joint applied research laboratory between the Naval Support and Experimentation Centre (Centro di Supporto e Sperimentazione Navale, CSSN) of the Italian Navy and the Italian Interuniversity Research Center of Integrated Systems for Marine Environment (ISME), who helped the research team during the missions at sea performed in La Spezia.

REFERENCES

Absil, P.A., Baker, C.G., and Gallivan, K.A. (2007). Trust-region methods on riemannian manifolds. *Foundations of Computational Mathematics*, 7(3), 303–330.

Bar-Shalom, Y., Li, X.R., and Kirubarajan, T. (2004). *Estimation with applications to tracking and navigation: theory algorithms and software*. John Wiley & Sons.

Cadena, C., Carlone, L., Carrillo, H., Latif, Y., Scaramuzza, D., Neira, J., Reid, I., and Leonard, J.J. (2016). Past, present, and future of simultaneous localization and mapping: Toward the robust-perception age. *IEEE Transactions on robotics*, 32(6), 1309–1332.

Caiti, A., Di Corato, F., Fenucci, D., Allotta, B., Costanzi, R., Monni, N., Pugi, L., and Ridolfi, A. (2014). Experimental results with a mixed USBL/LBL system for AUV navigation. In *2014 Underwater Communications and Networking (UComms)*, 1–4.

Chirikjian, G.S. (2011). *Stochastic models, information theory, and Lie groups, volume 2: Analytic methods and modern applications*, volume 2. Springer Science & Business Media.

Cieslak, P., Ridao, P., and Giergiel, M. (2015). Autonomous underwater panel operation by GIRONA500 UVMS: A practical approach to autonomous underwater manipulation. In *2015 IEEE International Conference on Robotics and Automation (ICRA)*, 529–536.

Costanzi, R., Monni, N., Ridolfi, A., Allotta, B., and Caiti, A. (2017). On field experience on underwater acoustic localization through USBL modems. In *OCEANS 2017 - Aberdeen*, 1–5.

Costanzi, R., Fanelli, F., Monni, N., Ridolfi, A., and Allotta, B. (2016). An attitude estimation algorithm for mobile robots under unknown magnetic disturbances. *IEEE/ASME Transactions on Mechatronics*, 21(4), 1900–1911.

Dellaert, F. (2012). Factor graphs and GTSAM: A hands-on introduction. Technical report, Georgia Institute of Technology.

Dellaert, F., Kaess, M., et al. (2017). Factor graphs for robot perception. *Foundations and Trends® in Robotics*, 6(1-2), 1–139.

Font, E.G., Bonin-Font, F., Negre, P.L., Massot, M., and Oliver, G. (2017). USBL integration and assessment in a multisensor navigation approach for AUVs 11this work is partially supported by ministry of economy and competitiveness under contracts tin2014-58662-r, dpi2014-57746-c3-2-r and feder funds. *IFAC-PapersOnLine*, 50(1), 7905–7910. 20th IFAC World Congress.

Forster, C., Carlone, L., Dellaert, F., and Scaramuzza, D. (2016). On-manifold preintegration for real-time visual–inertial odometry. *IEEE Transactions on Robotics*, 33(1), 1–21.

Franchi, M., Ridolfi, A., and Allotta, B. (2020). Underwater navigation with 2D forward looking SONAR: An adaptive unscented Kalman filter-based strategy for AUVs. *Journal of Field Robotics*.

Grisetti, G., Guadagnino, T., Aloise, I., Colosi, M., Della Corte, B., and Schlegel, D. (2020). Least squares optimization: From theory to practice. *Robotics*, 9(3), 51.

Gutmann, J.S. and Konolige, K. (1999). Incremental mapping of large cyclic environments. In *Proceedings 1999 IEEE International Symposium on Computational Intelligence in Robotics and Automation. CIRA'99 (Cat. No. 99EX375)*, 318–325. IEEE.

Kaess, M., Johannsson, H., Roberts, R., Ila, V., Leonard, J.J., and Dellaert, F. (2012). iSAM2: Incremental smoothing and mapping using the Bayes tree. *The International Journal of Robotics Research*, 31(2), 216–235.

Kaess, M., Ranganathan, A., and Dellaert, F. (2008). iSAM: Incremental smoothing and mapping. *IEEE Transactions on Robotics*, 24(6), 1365–1378.

Kim, J. (2020). Cooperative localization and unknown currents estimation using multiple autonomous underwater vehicles. *IEEE Robotics and Automation Letters*, 5(2), 2365–2371.

Kschischang, F.R., Frey, B.J., and Loeliger, H.A. (2001). Factor graphs and the sum-product algorithm. *IEEE Transactions on information theory*, 47(2), 498–519.

Leonard, J.J. and Bahr, A. (2016). Autonomous Underwater Vehicle navigation. In *Springer Handbook of Ocean Engineering*, 341–358. Springer.

Lu, F. and Milios, E. (1997). Globally consistent range scan alignment for environment mapping. *Autonomous robots*, 4(4), 333–349.

Morgado, M., Batista, P., Oliveira, P., and Silvestre, C. (2011). Position and velocity USBL/IMU sensor-based navigation filter. *IFAC Proceedings Volumes*, 44(1), 13642–13647. 18th IFAC World Congress.

Quigley, M., Conley, K., Gerkey, B., Faust, J., Foote, T., Leibs, J., Wheeler, R., and Ng, A.Y. (2009). ROS: an open-source Robot Operating System. In *ICRA workshop on open source software*, volume 3, 5. Kobe, Japan.

Vidal, E., Palomeras, N., Istenič, K., Hernández, J.D., and Carreras, M. (2019). Two-dimensional frontier-based viewpoint generation for exploring and mapping underwater environments. *Sensors*, 19(6).

Wang, J., Zhang, T., Jin, B., Zhu, Y., and Tong, J. (2020). Student's t-based robust Kalman filter for a SINS/USBL integration navigation strategy. *IEEE Sensors Journal*, 20(10), 5540–5553.

Wang, Y. and Chirikjian, G.S. (2008). Nonparametric second-order theory of error propagation on motion groups. *The International journal of robotics research*, 27(11-12), 1258–1273.

Westman, E. and Kaess, M. (2019). Degeneracy-aware imaging sonar simultaneous localization and mapping. *IEEE Journal of Oceanic Engineering*.